

Online design of experiments by active learning for nonlinear system identification

Kui Xie^a, Alberto Bemporad^a

^aIMT School for Advanced Studies Lucca, Lucca, Italy.

Abstract

We investigate the use of active-learning (AL) strategies to generate the input excitation signal at runtime for system identification of linear and nonlinear autoregressive and state-space models. We adapt various existing AL approaches for static model regression to the dynamic context, coupling them with a Kalman filter to update the model parameters recursively, and also cope with the presence of input and output constraints. We show the increased sample efficiency of the proposed approaches with respect to random excitation on different nonlinear system identification benchmarks.

Key words: Design of experiments, nonlinear system identification, active learning, extended Kalman filtering.

1 Introduction

Many system identification approaches exist, both for linear [22] and nonlinear systems [23, 27]. These methods typically rely on a given training dataset to estimate the model parameters that best approximate the system's behavior. Regardless of how well the model class is chosen or how advanced the method used to solve the training problem is, the quality of the identified model ultimately depends on the richness of the information contained in the training data. Relying solely on collecting more data can be costly, may introduce excessive redundancy without significantly increasing the information content, and complicate the optimization problem required to estimate the model parameters, due to the larger number of loss terms in the objective function to minimize [19, 26, 30].

The problem of optimal design of experiments (DoEs) has been studied for decades, dating back to the 1930s [11]. In the machine learning literature, the related problem of selecting the most informative samples to query for the target value is referred to as *active learning* (AL) [17, 32]. AL strategies aim to reduce the number of

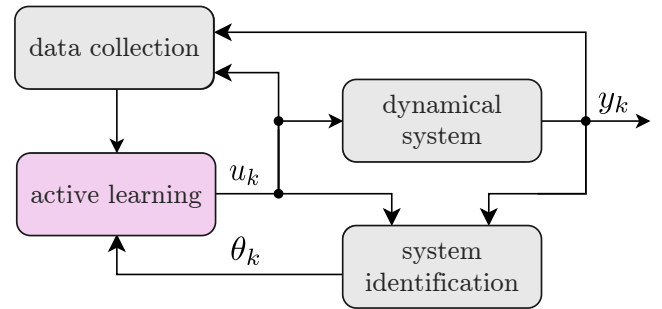


Fig. 1. Online active learning for system identification.

required training samples by allowing the training algorithm to select the feature vectors to query. Several AL methods have been proposed in the literature, primarily for classification problems [1], although contributions also exist for regression tasks [2, 5, 7, 9, 13, 20, 25, 38]. Such methods mainly focus on learning *static* models to explain the relationship between feature vectors and targets. The samples can be arbitrarily selected from a dense set of admissible values, a pre-determined discrete pool, or a stream of feature-vector samples [32]. However, actively learning *dynamical* models is a more challenging task because not all the components of the feature vector can be changed instantaneously. Research on AL for system identification is therefore limited, and it is primarily restricted to specific classes of models such as Gaussian processes [34, 42], linear parameter-varying models [8], autoregressive models [39], nonlinear state-space models [15], and neural-network state-space models [24]. Furthermore, these approaches assume that the

Email addresses: kui.xie@imtlucca.it (Kui Xie), alberto.bemporad@imtlucca.it (Alberto Bemporad).

¹ This paper was not presented at any IFAC meeting. This research was supported by the European Research Council (ERC), Advanced Research Grant COMPACT (Grant Agreement No. 101141351). Corresponding author K. Xie.

state x_k is measurable, while often only input/output data are available for system identification.

1.1 Contribution

We extend the AL methods reported in [2, 5, 28, 38, 41] for the regression of static functions to the dynamic context, focusing on learning black-box parametric models from input/output data. Specifically, we consider the problem of identifying autoregressive models, either linear (ARX) or nonlinear (NARX), and state-space models in recurrent neural network (RNN) form. A schematic diagram of the proposed strategy is shown in Fig. 1: each time a new input sample u_k is generated by the AL algorithm and an output sample y_k is acquired, we update the model parameters θ_k via a linear or extended Kalman filter (EKF) [3, 21], depending on the chosen model class.

The proposed recursive approach employs online optimization, based on the data collected so far, to design the experiment at runtime. As for supervised AL of static models, the developed DoE strategies ensure that the collected data are informative and diverse [32], i.e., respectively, are acquired to minimize modeling errors and explore the state/action space, trying to avoid repetitions. Based on the AL method for regression proposed in [2], we use an acquisition method based on a non-probabilistic measure of the uncertainty associated with output predictions to sample the system where uncertainty is expected to be most significant, and employ inverse-distance weighting (IDW) functions to ensure the exploration of areas not visited before. Related online AL algorithms have been proposed recently for improving the sample efficiency of reinforcement learning (RL) [18], model predictive coverage control [29], Bayesian optimization (BO) [33, 40], latent space dynamics identification [12], covariance steering [16], and deep metric learning [36].

We consider both one-step-ahead AL formulations, based on the uncertainty associated with the following predicted output, and a less myopic multi-step-ahead AL approach, based on the uncertainty related to the predicted outputs over a finite horizon. Moreover, we also take into account the presence of input and output constraints, with the latter treated as soft to avoid excessive conservativeness, especially at early stages when the model is very uncertain. The online computation effort of the proposed AL algorithm is limited, in particular, when the input can be selected from a discrete set (e.g., as in the case of pseudo-random binary signal excitation, where the set has only two elements). However, if the sampling frequency used to collect data is too high for real-time optimization, our algorithm can still be applied to a digital twin. In this case, the input sequence generated during the simulation can be saved and later used to excite the actual process.

Compared to our conference paper [39], in this paper we introduce several key improvements. Besides considering more complex NARX models, such as small-scale neural networks, we extend the AL methods to *state-space* models, including RNN-based models, which pose additional challenges due to the presence of hidden states. We also validate the proposed algorithms on a much broader range of practical examples, demonstrating their effectiveness compared to random excitation in a set of realistic scenarios.

The paper is structured as follows. In Sections 2 and 3, we present the proposed algorithm for NARX models and state-space models, respectively. Numerical experiments on nonlinear state-space models are reported in Section 4. Finally, conclusions are drawn in Section 5.

2 Active Learning of NARX Models

We first consider the problem of identifying a strictly-causal NARX model in the form

$$\hat{y}_k = f(x_{k-1}, \theta) \quad (1a)$$

$$x_{k-1} = [y'_{k-1} \ \dots \ y'_{k-n_a} \ u'_{k-1} \ \dots \ u'_{k-n_b}]' \quad (1b)$$

where $\hat{y}_k \in \mathbb{R}^{n_y}$, $u_k \in \mathbb{R}^{n_u}$, $n_a \geq 0$, $n_b \geq 0$, $\theta \in \mathbb{R}^{n_\theta}$ is the vector of parameters to learn, and $k = -\max\{n_a, n_b\}, -\max\{n_a, n_b\} + 1, \dots, 0, 1, \dots$ is the sample index. For example, f could be a linear model, $f(x, \theta) = \theta'x$, or a small-scale neural network with weights and bias terms collected in θ . Our goal is to *actively* generate control inputs u_k at runtime, $k = 0, 1, \dots, N - 1$, to efficiently learn the parameter vector θ , solving the posed system identification problem in a sample-efficient manner.

From now on, we assume that all input and output signals are properly scaled. In particular, we assume the *standard scaling* transformation

$$\sigma(\alpha) = \frac{\alpha - \mu_\alpha}{\sigma_\alpha} \quad (2)$$

where $(\mu_\alpha, \sigma_\alpha)$ denote the mean and standard deviation of the signal α , are applied on input and output signals, whose means and standard deviations — denoted as μ_u, σ_u for the input and μ_y, σ_y for the output, respectively — are assumed to be known.

In the sequel, we will denote by θ_k the model parameter vector obtained by training the model with the outputs collected up to time k and inputs up to time $k - 1$. As in most practical applications, we assume that the input u_k is subject to the constraint $u_k \in \mathcal{U}$, where \mathcal{U} is the set of valid inputs. For instance, the hyper-box $\mathcal{U} = \{u \in \mathbb{R}^{n_u} : u_{\min} \leq u \leq u_{\max}\}$ or, in alternative, a finite set $\mathcal{U} = \{u^1, \dots, u^M\}$, $u^j \in \mathbb{R}^{n_u}$, $j = 1, \dots, M$, such as $\mathcal{U} = \{-1, 1\}$ in the case of scalar pseudorandom binary sequence excitation.

2.1 One-step-ahead active learning

Consider any *acquisition function* $a : \mathbb{R}^{n_x} \rightarrow \mathbb{R}$ for solving an AL problem for regression [32] (as shown later, a will change with the sample time k , in general), where n_x is the number of features; in this case, $n_x = n_a n_y + n_b n_u$ is then number of past input and outputs

$$x_k \triangleq [y'_k \dots y'_{k-n_a+1} \ u'_k \ u'_{k-1} \dots u'_{k-n_b+1}]'$$

used in the NARX representation (1). Ideally, given a new measurement y_k , we would like to choose

$$x_k = \arg \max_x a(x).$$

However, at time k , the only component in x_k that can be freely chosen is the current input u_k , given that all the remaining components involve outputs and inputs already measured. Hence, we restrict the acquisition problem to

$$u_k = \arg \max_{u \in \mathcal{U}} a(x_k(u)) \quad (3a)$$

$$x_k(u) \triangleq [y'_k \dots y'_{k-n_a+1} \ u' \ u'_{k-1} \dots u'_{k-n_b+1}]' \quad (3b)$$

where $x_k : \mathbb{R}^{n_u} \rightarrow \mathbb{R}^{n_x}$ defines the feature vector corresponding to a given input selection. Note that when the input u_k is chosen from a finite set $\mathcal{U} = \{u^1, \dots, u^M\}$, problem (3a) can be easily solved by enumeration, analogously to *pool-based* active learning algorithms [32]. The new input u_k and measured output y_{k+1} can be immediately used to update the model parameters θ_{k+1} . In this paper, we use an EKF to update θ_{k+1} or simply a linear Kalman filter in case $f(x_{k-1}, \theta) = \theta' \bar{f}(x_{k-1})$ defines a linear ARX model. Generally, the acquisition function $a(x)$ optimized in (3a) depends on θ_k and all the past feature-vector/target samples (x_{k-1}, y_k) collected up to step k .

In [2], the author proposed an AL method for regression, called *ideal*, based on inverse distance weighting (IDW) functions, that we briefly review here and slightly extend for experiment design. Let us define the squared inverse weighting functions² $w_j : \mathbb{R}^{n_x} \rightarrow \mathbb{R}$

$$w_j(x) = \frac{1}{d^2(x, x_j)}, \quad j = 0, \dots, k$$

where the function $d^2(x, x_j) = \|x_j - x\|^2$ measures the squared Euclidean distance between (the scaled) vectors

² Alternatively, we can use $w_j(x) = e^{-d^2(x, x_j)}/d^2(x, x_j)$ to let the weight to decay more quickly as the distance of x from x_j gets larger.

x and x_j . Let $v_j : \mathbb{R}^n \rightarrow \mathbb{R}$ be defined for $j = 0, \dots, k$ as

$$v_k(x) = \begin{cases} 1 & \text{if } x = x_j \\ 0 & \text{if } x = x_h, \ h \neq j \\ \frac{w_j(x)}{\sum_{h=1}^k w_h(x)} & \text{otherwise.} \end{cases}$$

The acquisition function consists of two non-negative terms:

$$a(x) = s^2(x) + \delta z(x) \quad (4)$$

where the *IDW variance* function

$$s^2(x) = \sum_{j=0}^k v_j(x) \|y_j - f(x_{j-1}, \theta_k)\|_2^2 \quad (5)$$

is a proxy for the variance of the output y predicted by the model at x , $z(x)$ is the *IDW exploration* function,

$$z(x) = \begin{cases} 0 & x \in \{x_0, \dots, x_k\} \\ \frac{2}{\pi} \tan^{-1} \left(\frac{1}{\sum_{j=0}^k w_j(x)} \right) & \text{otherwise} \end{cases} \quad (6)$$

and $\delta \geq 0$ is a trade-off coefficient between exploitation (of the model θ_k , used to estimate model uncertainty) and pure exploration (since $z(x) = 0$ at each x_j sampled so far, $j = 0, \dots, k$).

Besides *ideal*, we will consider also the following alternative incremental AL methods: the greedy method GS_x [41, Algorithm 1], the greedy method iGS [38, Algorithm 3], and the query-by-committee method QBC [5, 28]. We exclude the iRDM method [20] as it cannot be used for recursive model learning. See [2, Section 3.4] for a review of these methods for regression of static models. See Section 2.4 below for the adaptation of GS_x , iGS , and QBC to the dynamic context.

2.2 Initialization

As typically done in most AL algorithms, we start by using *passive* learning to gather N_i initial pairs of input/output samples, $N_i \geq 0$. The simplest approach is to use random sampling, that is, to generate u_0, \dots, u_{N_i-1} randomly (cf. [2, Section 3.1]).

Remark 1. It is well known that closed-loop system identification data — where the input u_k depends on past outputs — can introduce bias in model estimation if not properly addressed. The input u_k our AL method chooses by solving (3) depends on past output measurements, due to $x_k(u)$. However, in our approach, the pure exploration term $z(x_k(u))$ (6) is exactly designed to ensure sufficient excitation and diversity in the data, thereby mitigating the risk of bias commonly associated with closed-loop identification. While our current model

adaptation relies on (extended) Kalman filtering, classical techniques such as instrumental variables (IV) could also be incorporated to further address potential closed-loop effects, an interesting direction for future work.

2.3 Constraints

To attempt satisfying also *output* constraints, we add a penalty in (3a) on the expected violation of output constraints. For instance, the satisfaction of output constraints

$$y_{\min} \leq y \leq y_{\max} \quad (7)$$

can be encouraged by introducing the penalty term

$$p(x) = \rho \sum_{i=1}^{n_y} \{ \max\{\hat{y}_{k+1,i}(x, \theta_k) - y_{\max,i}, 0\} + \max\{y_{\min,i} - \hat{y}_{k+1,i}(x, \theta_k), 0\} \} \quad (8)$$

where $\hat{y}_{k+1} = f(x, \theta_k)$ is the next output predicted by the current model with parameter vector θ_k , and ρ is a penalty parameter, $\rho \geq 0$. Then, we solve the following problem

$$u_k = \arg \max_{u \in \mathcal{U}} a(x_k(u)) - p(x_k(u)). \quad (9)$$

A drawback of using the penalty term (8) is that it does not account for model uncertainty, which might be quite large during the early phase of sampling. To address this issue, we consider the confidence interval proposed in [14] for IDW functions, which is defined as

$$\hat{y}_{k+1}(x, \theta_k) \pm \kappa_\alpha s(x) \quad (10)$$

where $s(x)$ is the square root of the IDW variance function $s^2(x)$ (5) and the scaling factor κ_α is set as the upper α sample quantile of

$$\frac{|CV_i|}{s_{-(i-1)}(x_{i-1})}, \quad i = 0, \dots, k$$

where α is a constant, typically set to 90%, $CV_i = y_i - \hat{y}_i(x_{i-1}, \theta_k)$ is the cross-validation error at x_{i-1} , $s_{-i}^2(x_i) = \sum_{j=0, j \neq i}^k v_{j(i)}(x_i)(y_j - \hat{y}_{i+1}(x_i, \theta_k))$, $v_{j(i)}(x_i) = w_j(x_i) / \sum_{l=0, l \neq i}^k w_l(x_i)$, and $w_l(x)$ is the weighting function. To prevent over-shrinking the constraint set in (9), we impose a limit on the quantity $\kappa_\alpha s(x) \leq \beta(y_{\max} - y_{\min})$, where, in this case, we set $\beta = \frac{1}{3}$. Finally, in (9) we take into account the uncertainty of output predictions by replacing $p(x)$ with

$$p(x) = \rho \sum_{i=1}^{n_y} \{ \max\{\hat{y}_{k+1,i}(x, \theta_k) - y_{\max,i} + \kappa_\alpha s(x), 0\} + \max\{y_{\min,i} - \hat{y}_{k+1,i}(x, \theta_k) + \kappa_\alpha s(x), 0\} \}. \quad (11)$$

2.4 Alternative active-learning methods

We review three different AL methods for regression, alternative to *ideal*, slightly adapted here to generate input signals for system identification.

2.4.1 Greedy method GS_x

The method GS_x [41, Algorithm 1] selects the next sample x_k by maximizing its minimum distance from the existing samples. This method is not model-based, as it only aims to fill the input space.

In analogy with (9), we extend GS_x based on the acquisition problem

$$u_k = \arg \max_{u \in \mathcal{U}} d_x(x_k(u)) - p(x_k(u))$$

where $d_x(x) = \min_{i=0}^k \|x - x_i\|_2^2$ is the minimum distance from existing samples.

2.4.2 Greedy method iGS

Given the predictor $f(x_k(u), \theta_k)$ trained on the available samples, the greedy sampling technique iGS [38, Algorithm 3] selects the next input u_k by solving the acquisition problem

$$u_k = \arg \max_{u \in \mathcal{U}} d_x(x_k(u)) d_y(x_k(u)) - p(x_k(u))$$

where $d_x(x)$ is the same as in GS_x and $d_y(x) = \min_{i=0}^k \|\hat{y}_{k+1}(x, \theta_k) - y_i\|_2^2$ is the predicted minimum distance in the output space from existing output samples.

2.4.3 Query-by-Committee method QBC

The Query-by-Committee (QBC) method for regression [5, 28] utilizes K_{QBC} different predictors θ_k^j , $j = 1, \dots, K_{QBC}$. In AL of static models, the predictors are typically obtained by bootstrapping the acquired dataset. In contrast, as we acquire the samples online, we create K_{QBC} different models by running K_{QBC} (extended) Kalman filters in parallel and, at each time step, only update $K_{QBC} - 1$ models after acquiring the new sample y_k to diversify them. This adaptation of QBC aims at choosing the input u_k that maximizes the variance of the estimated output prediction $\hat{y}_{k+1}(x_k(u), \theta_k^j)$:

$$u_k = \arg \max_{u \in \mathcal{U}} \sum_{j=1}^{K_{QBC}} \left\| \hat{y}_{k+1}(x_k(u), \theta_k^j) - \frac{\sum_{h=1}^{K_{QBC}} \hat{y}_{k+1}(x_k(u), \theta_k^h)}{K_{QBC}} \right\|_2^2 - p(x_k(u)). \quad (12)$$

Algorithm 1 Online design of experiments for system identification of NARX models using active learning and inverse-distance based exploration (ideal-sysid-NARX).

Input: Set \mathcal{U} of admissible inputs, number N_i of passively-sampled inputs, length N of the experiment to design, exploration hyperparameter $\delta \geq 0$, number $L \geq 1$ of prediction steps, possible upper and lower bounds y_{\max}, y_{\min} , penalty parameter $\rho \geq 0$ on output constraint violations, number N_e of epochs used to train the initial model via EKF.

1. Generate N_i samples u_0, \dots, u_{N_i-1} by passive learning (e.g., random sampling);
2. Excite the system and collect y_0, \dots, y_{N_i-1} ;
3. Estimate θ_{N_i-1} by running EKF N_e times;
4. **For** $k = N_i, \dots, N$ **do**:
 - 4.1. measure y_k ;
 - 4.2. update θ_k by (extended) Kalman filtering;
 - 4.3. **If** $k < N$, get u_k by solving problem (13), with penalty p as in (8) or (11) to handle possible output constraints;
5. **End.**

Output: Estimated parameter vector θ_N ; input excitation u_0, \dots, u_{N-1} .

2.5 Multi-step prediction

So far, we only considered one-step-ahead predictions \hat{y}_{k+1} to choose the next control input u_k . To circumvent such a possible myopic view, we can take a *predictive* approach and extend the formulation (9) to optimize a finite sequence of future inputs $U_k = [u'_k \ u'_{k+1} \ \dots \ u'_{k+L-1}]'$,

$$U_k = \arg \max_{U \in \mathcal{U}^L} \sum_{j=0}^{L-1} (a(x_{k+j}(U)) - p(x_{k+j}(U)))$$

where $L \geq 1$ is the desired prediction horizon and $\mathcal{U}^L \triangleq \mathcal{U} \times \dots \times \mathcal{U}$. In this case, the predicted regressor vector x_{k+j} entering the acquisition function a contains either outputs \hat{y}_{k+h} predicted by model θ_k ($h \geq 1$) or measured outputs y_{k+h} ($h \leq 0$), and either current/future inputs u_{k+h} ($h \geq 0$) to be optimized or past inputs (for $h < 0$). Note that, by causality, the predicted regressor as $x_{k+j}(U)$ only depends on the first $j+1$ inputs in U .

In the case we use the ideal acquisition function, since future measured outputs y_{k+j+1} are not available, replacing them by surrogates $\hat{y}_{k+j+1} = f(\hat{x}_{k+j}, \theta_k)$ cause the IDW variance $s^2(\hat{x}_{k+j}) = 0$, and thus $a(\hat{x}_{k+j}) = z(\hat{x}_{k+j})$, $\forall j > 0$. Therefore, the multi-step-ahead active learning problem becomes:

$$U_k = \arg \max_{U \in \mathcal{U}^L} s^2(x_k(U)) + \delta \sum_{j=0}^{L-1} (z(x_{k+j}(U)) - p(x_{k+j}(U))). \quad (13)$$

Note that (13) coincides with (9) when $L = 1$ as $x_k(U) = x_k(u)$.

Based on the receding-horizon mechanism used in model predictive control, after solving (13), only the current input u_k is applied to excite the process, while the remaining moves u_{k+j} are discarded, for all $j = 1, \dots, L-1$. Then, after acquiring the new measurement y_{k+1} and updating the model to get the new parameter vector θ_{k+1} , problem (13) is solved again to get U_{k+1} , and so on.

The overall algorithm for online input design for NARX model system identification based on the ideal active learning approach, denoted by ideal-sysid-NARX, is summarized in Algorithm 1.

2.6 Numerical complexity

To analyze the complexity of Algorithm 1, we assume that the model parameter vector θ is estimated using EKF, which has complexity $O(n_\theta^2)$ per step, mainly due to covariance matrix updates. The initial batch training via EKF run N_e times at Step 3 over N_i samples contributes $O(n_\theta^2 N_e N_i)$ operations, and the recursive parameter estimation contributes further $O(n_\theta^2 (N - N_i))$ operations at Step 4.2. For QBC, $(K_{QBC} - 1)$ additional EKF instances increase the parameter estimation cost to $O(K_{QBC} n_\theta^2 N)$.

For pool-based sampling with $\mathcal{U} = \{u^1, \dots, u^M\}$, solving problem (13) requires $(N - N_i)M^L$ evaluations of the acquisition function $a(x)$, or $(N - N_i)M$ for single-step prediction ($L = 1$) at Step 4.3. Each evaluation of (4) involves computing IDW weights and distances to all previous samples, with complexity $O(k)$ at iteration k , yielding total complexity $O(MN^2)$ for the acquisition function evaluations. Model predictions require $(N - N_i)ML$ evaluations of the NARX model (1), each with cost C_f , and constraint handling via (8) adds $(N - N_i)ML$ penalty function evaluations. Hence, the overall computational complexity is $O(n_\theta^2 (N + N_e N_i) + MN^2 + MNLC_f)$.

3 Active Learning of State-Space Models

The procedures presented in the previous section can be extended to learn strictly causal³ state-space models of the form

$$\begin{aligned} x_{k+1} &= f_x(x_k, u_k, \theta_x) \\ y_k &= f_y(x_k, \theta_y) \end{aligned} \quad (14)$$

where $x_k \in \mathbb{R}^{n_x}$ is now the hidden state vector at time k . Here, we focus on RNN models, in which f_x, f_y are feedforward neural networks with weights and bias terms

³ The approach can be extended to non-strictly causal models with some modifications to handle the presence of I/O feedthrough.

collected in θ_x, θ_y , respectively, although the approach can be applied to any parametric nonlinear state-space model. In order to actively learn model (14), we must explore the space of state-input vectors $q_k = [x'_k, u'_k]'$. However, as in the case of NARX models, only the component u_k of q_k can be decided arbitrarily at time k . Given that the hidden state x_k is not modifiable (and even not measurable), we must consider its estimate $x_{k|k}$ at time k . Such an estimate depends on the past information $I_k \triangleq \{u_0, \dots, u_{k-1}, y_0, \dots, y_k\}$.

Consider the current time k and let the current model-coefficient vectors $\theta_{x|k}, \theta_{y|k}$ be estimated from I_k . Let $x_{0|k}, \dots, x_{k|k}$ be the sequence of hidden states estimated by reprocessing the dataset I_k in accordance with (14) with $\theta_x = \theta_{x|k}, \theta_y = \theta_{y|k}$; in particular, as suggested in [4, Section III.C], we run an extended Kalman filter (or a linear Kalman filter, in case model (14) is linear) and Rauch-Tung-Striebel (RTS) smoothing [31, p. 268] to get $x_{0|k}$, further refine $x_{0|k}$ by nonlinear programming (L-BFGS optimization), and run EKF to get the following states $x_{1|k}, \dots, x_{k|k}$. Then, similarly to (3a), we solve the acquisition problem

$$u_k = \arg \max_{u \in \mathcal{U}} a \left(\begin{bmatrix} x_{k|k} \\ u \end{bmatrix} \right)$$

where the acquisition function a depends on the active-learning method used, as described next.

Greedy method GS_x. The input u_k is obtained by solving

$$u_k = \arg \max_{u \in \mathcal{U}} d_x \left(\begin{bmatrix} x_{k|k} \\ u \end{bmatrix} \right)$$

where $d_x(q) = \min_{i=0, \dots, k-1} \|q - q_i\|_2^2$ and $q_i = [x'_{i|k}, u'_i]'$ is the vector collecting existing state estimates and past input samples.

Greedy method iGS. We select the input u_k as

$$u_k = \arg \max_{u \in \mathcal{U}} d_x \left(\begin{bmatrix} x_{k|k} \\ u \end{bmatrix} \right) \cdot d_y \left(\begin{bmatrix} f_y(f_x(x_{k|k}, u, \theta_{x|k}), \theta_{y|k}) \\ f_x(x_{k|k}, u, \theta_{x|k}) \end{bmatrix} \right)$$

where $d_y(r) = \min_{i=0, \dots, k-1} \|r - r_i\|_2^2$ is the minimum distance in the state and output space from predicted states and existing output samples and $r_i = [y'_{i+1}, x'_{i+1|k}]'$ is the vector collecting past output measurements and state estimates.

Method ideal. Similarly to (3a) the input u_k is obtained by solving

$$u_k = \arg \max_{u \in \mathcal{U}} s^2(q) + \delta z(q)$$

where $z(q)$ is the IDW function (6) defined over the samples q_i , and the IDW variance function s^2 similar to (5) is defined as

$$s^2(q) = \sum_{j=0}^{k-1} v_j(q) (\|f_y(f_x(q_x, q_u, \theta_{x|k}), \theta_{y|k}) - y_{j+1}\|_2^2 + \alpha \|f_x(q_x, q_u, \theta_{x|k}) - x_{j+1|k}\|_2^2). \quad (15)$$

In (15), we split $q = [q'_x, q'_u]'$ and $v_j(q)$ are the IDW coefficient functions defined over the same samples q_i . The coefficient $\alpha > 0$ trades off between emphasizing the uncertainty associated with the outputs and the one associated with the states.

QBC method. We use the same formulation as in (12), but with the predicted output $\hat{y}_{k+1}(q, \theta_{y|k}^j) = f_y(f_x(q_x, q_u, \theta_{x|k}^j), \theta_{y|k}^j)$.

For the safe exploration of the output space, like in the NARX case (9), we can add a penalty term to the acquisition function and solve the following problem

$$u_k = \arg \max_{u \in \mathcal{U}} a(q) - p(q) \quad (16a)$$

where

$$p(q) = \rho \sum_{i=1}^{n_y} \{ \max\{\hat{y}_{k+1,i}(q, \theta_{y|k}) - y_{\max,i}\}, 0 \} + \max\{y_{\min,i} - \hat{y}_{k+1,i}(q, \theta_{y|k}), 0\} \quad (16b)$$

and $\hat{y}_{k+1}(q, \theta_{y|k}) = f_y(f_x(q_x, q_u, \theta_{x|k}), \theta_{y|k})$ is the predicted output at the next time step $k+1$ given the current state estimate $x_{k|k}$ and the input u .

A multi-step ahead version of the active learning problem can be formulated for state-space models too, similarly to the NARX case, only using the IDW variance function s^2 for the first step and the IDW exploration function z at all future steps in prediction, where future samples, $q_{k+j} = [x'_{k+j|k}, u'_{k+j}]'$, are predicted by running the model with the current coefficients $\theta_{x|k}, \theta_{y|k}$ in open-loop.

The overall algorithm for online input design for state-space model system identification based on the ideal active learning approach, denoted by **ideal-sysid-SS**, is summarized in Algorithm 2. The model is initially trained by L-BFGS-B [6] via the **jax-sysid** package [4] and then refined recursively using EKF after each active-learning step. Algorithm 2 is also applied using the other acquisition functions **GS_x**, **iGS**, and **QBC**.

Algorithm 2 Online design of experiments for system identification of state-space models using active learning and inverse-distance based exploration (*ideal-sysid-SS*).

Input: Set \mathcal{U} of admissible inputs, number N_i of passively-sampled inputs, length N of the experiment to design, exploration hyperparameters $\delta, \alpha \geq 0$, number $L \geq 1$ of prediction steps, possible upper and lower bounds y_{\max}, y_{\min} , penalty parameter $\rho \geq 0$ on output constraint violations, state-sequence reconstruction interval $m \geq 1$, number N_b of epochs used to train the initial model via L-BFGS-B.

1. Generate N_i samples u_0, \dots, u_{N_i-1} by passive learning (e.g., random sampling)
 2. Excite the system and collect y_0, \dots, y_{N_i-1} ;
 3. Initialize model parameters $\bar{\theta}_{N_i-1}$ by L-BFGS-B N_b times on collected training data;
 4. Run (extended) Kalman filter to refine estimate θ_{N_i-1} and initialize covariance matrices;
 5. Reconstruct $\hat{x}_0, \hat{x}_1, \dots, \hat{x}_{N_i}$ by EKF and RTS smoothing plus L-BFGS refinement;
 6. **For** $k = N_i, \dots, N$ **do**:
 - 6.1. measure y_k ;
 - 6.2. update θ_k by (extended) Kalman filtering;
 - 6.3. (only every m steps) reconstruct $\hat{x}_0, \hat{x}_1, \dots, \hat{x}_{k+1}$ by EKF and RTS smoothing + L-BFGS refinement;
 - 6.4. **If** $k < N$, get u_k by solving problem (16);
 7. **End.**
-

Output: Estimated parameter vector θ_N ; input excitation u_0, \dots, u_{N-1} .

3.1 Numerical complexity

In analyzing the complexity of Algorithm 2, we assume that the model parameters θ_x and θ_y are initially estimated using N_b L-BFGS-B iterations at Step 3, with complexity $O((n_{\theta_x} + n_{\theta_y})N_b N_i C_{f_x, f_y} + (n_{\theta_x} + n_{\theta_y})^2 N_b)$, where the first term accounts for gradient computation through backpropagation and the second for L-BFGS-B parameter updates. Here, C_{f_x, f_y} represents the cost of evaluating the state-space model (14). Subsequently, refining the estimate using EKF at Step 4 and recursive parameter estimation at Step 6.2 contributes $O((n_{\theta_x} + n_{\theta_y})^2 N)$ operations.

A key difference from the NARX case is the state reconstruction at Step 6.3: every m iterations, all past states $\hat{x}_0, \dots, \hat{x}_{k+1}$ must be reconstructed based on the latest model using EKF forward pass and RTS smoothing, requiring $O(n_x^2 k)$ operations at each iteration k , leading to a total $O(n_x^2 N^2 / m)$ operation complexity.

For pool-based sampling, the acquisition function evaluation at Step 6.4 follows the same pattern as the NARX case, requiring $(N - N_i)M$ evaluations for single-step prediction ($L = 1$). However, the feature vectors now include predicted states $q_k = [x'_k, u'_k]'$, and the IDW computations operate in this augmented space with

complexity $O(k)$ at iteration k , yielding total complexity $O(MN^2)$. Model predictions require evaluating the state-space model (14), with $(N - N_i)ML$ total evaluations, and constraint handling via (8) adds $(N - N_i)ML$ penalty function evaluations.

The overall computational complexity is $O((n_{\theta_x} + n_{\theta_y})N_b N_i C_{f_x, f_y} + (n_{\theta_x} + n_{\theta_y})^2(N + N_b) + (n_x^2 N^2)/m + MN^2 + MNLC_{f_x, f_y})$. The state reconstruction term $O(n_x^2 N^2 / m)$ may dominate for high-dimensional states, especially when $m = 1$ (reconstruction at every step). This makes *ideal-sysid-SS* computationally more intensive than *ideal-sysid-NARX*, where state reconstruction is not required.

4 Numerical Experiments

We assess the performance of the proposed active learning algorithms on both NARX neural network (NARX-NN) models, using Algorithm 1 (*ideal-sysid-NARX*), and RNN state-space models, using Algorithm 2 (*ideal-sysid-SS*), across three standard nonlinear system identification benchmarks: a two-tank system [35], an ethylene oxidation plant [10], and an industrial robot arm [37]. For comparison, we also include passive learning and alternative active learning methods (GS_x, iGS) as described in Sections 2.4 and 3. The QBC method has been implemented and tested, but is not reported in the experiments due to its poor performance, even when compared to passive sampling.

4.1 Experimental Setup

For each benchmark, noisy synthetic data are generated by numerically integrating the underlying system of nonlinear ordinary differential equations of the plant model with high accuracy. All methods use N_i initial samples generated by random sampling, with standard scaling (2) applied to input/output data based on statistics from the initial dataset.

The main differences between NARX-NN and RNN settings are summarized as follows:

Covariance matrices. For NARX-NN models, EKF only estimates the neural network parameters. In this context, $Q_\theta \in \mathbb{R}^{n_\theta \times n_\theta}$ and $R \in \mathbb{R}^{n_y \times n_y}$ are hyperparameters of the EKF representing the covariance matrices of process and measurement noise, respectively, and $P_k \in \mathbb{R}^{n_\theta \times n_\theta}$ is the resulting covariance matrix of parameter estimation errors. For RNN-based models, EKF estimates both the parameters and the hidden states of the RNN. The covariance matrix $\bar{Q}_x \in \mathbb{R}^{n_x \times n_x}$ of state noise is a further hyperparameter. The resulting matrix $\bar{P}_k \in \mathbb{R}^{(n_x + n_{\theta_x} + n_{\theta_y}) \times (n_x + n_{\theta_x} + n_{\theta_y})}$ is the covariance matrix of the combined state and parameter estimation errors.

Model training. NARX-NN parameters $\theta \in \mathbb{R}^{n_\theta}$ are initially trained by running EKF $N_e = 50$ times over the same data. RNN parameters θ_x and θ_y are first trained by L-BFGS-B using `jax-sysid` [4] and then refined using EKF. Both models are subsequently updated recursively via EKF.

State estimation. NARX-NN models do not require estimating hidden states, whereas for RNNs, hidden states are estimated at each step using EKF and RTS smoothing as required by the AL methods. As the model parameters θ_k changes relatively slowly, we only re-estimate the entire sequence of past hidden states $\hat{x}_0, \dots, \hat{x}_k$ every m steps, with $m = 10$. We found that this does not affect the performance of the AL methods significantly.

In the following examples, all neural network models share similar structures. Specifically, the first prediction model $f(x_{k-1}, \theta_k)$ is the two-layer NARX neural network

$$f(x_{k-1}, \theta_k) = W_3 \sigma_2(W_2 \sigma_1(W_1 x_{k-1} + b_1) + b_2) + b_3 \quad (17)$$

where $x_{k-1} \in \mathbb{R}^{n_x}$ is the regressor vector, $n_x = n_a + n_b$, $n_a = 3$, $n_b = 3$, $n_u = 1$, $n_y = 1$, $W_1 \in \mathbb{R}^{n_1 \times n_x}$, $b_1 \in \mathbb{R}^{n_1}$, $W_2 \in \mathbb{R}^{n_2 \times n_1}$, $b_2 \in \mathbb{R}^{n_2}$, $W_3 \in \mathbb{R}^{n_y \times n_2}$, and $b_3 \in \mathbb{R}^{n_y}$. The activation functions $\sigma_1(\cdot)$ and $\sigma_2(\cdot)$ are elementwise arctan functions. The parameter vector θ_k collects all weights and bias terms.

The RNN model used for the identification of state-space models consists of the following state-update f_x and output function f_y :

$$f_x(x_k, u_k, \theta_x) = W_3^x \sigma_2(W_2^x \sigma_1(W_1^x [x_k' u_k']' + b_1^x) + b_2^x) + b_3^x \quad (18a)$$

$$f_y(x_k, \theta_y) = W_2^y \sigma_3(W_1^y x_k + b_1^y) + b_2^y \quad (18b)$$

where $[x_k' u_k']' \in \mathbb{R}^{n_x + n_u}$ is the concatenated state and input vector. The matrices $W_1^x \in \mathbb{R}^{n_1^x \times (n_x + n_u)}$, $W_2^x \in \mathbb{R}^{n_2^x \times n_1^x}$, $W_3^x \in \mathbb{R}^{n_x \times n_2^x}$ and vectors $b_1^x \in \mathbb{R}^{n_1^x}$, $b_2^x \in \mathbb{R}^{n_2^x}$, $b_3^x \in \mathbb{R}^{n_x}$ are the weights and biases of the state-update network, with $\sigma_1(\cdot)$ and $\sigma_2(\cdot)$ being elementwise tanh activation functions. The output network uses $W_1^y \in \mathbb{R}^{n_1^y \times n_x}$, $W_2^y \in \mathbb{R}^{n_y \times n_1^y}$, $b_1^y \in \mathbb{R}^{n_1^y}$, $b_2^y \in \mathbb{R}^{n_y}$, and an elementwise tanh activation $\sigma_3(\cdot)$. The parameter vectors θ_x and θ_y collect all weights and biases of the state-update and output networks, respectively.

Performance is evaluated using one-step-ahead prediction ($L = 1$). The overall prediction quality on training and test datasets is quantified using the root-mean-square error (RMSE), defined as

$$\text{RMSE} = \sqrt{\frac{1}{N_{\max}} \sum_{k=0}^{N_{\max}-1} (y_k - \hat{y}_k)^2}$$

where $\hat{y}_k = f(x_{k-1}, \hat{\theta}_k)$ for NARX-NN models, while $\hat{y}_k = f_y(\hat{x}_k, \hat{\theta}_{y|k})$ for RNNs, and N_{\max} is the number of samples in the set ($N_{\max} = N$ for training and $N_{\max} = N_{\text{test}}$ for testing). Model quality is also assessed by the R^2 coefficient of determination, defined as

$$R^2 = \left(1 - \frac{\sum_{k=0}^{N_{\max}-1} (y_k - \hat{y}_k)^2}{\sum_{k=0}^{N_{\max}-1} (y_k - \bar{y})^2} \right) \times 100\% \quad (19)$$

where $\bar{y} = \frac{1}{N_{\max}} \sum_{k=0}^{N_{\max}-1} y_k$ is the mean of the output data. To quantify output constraint violations (7), we report the mean constraint violation (MCV) over N_r runs:

$$\text{MCV} = \frac{\sum_{j=1}^{N_r} \sum_{k=N_i}^N \max(0, y_k^j - y_{\max}, y_{\min} - y_k^j)}{N_r(N - N_i)} \quad (20)$$

where y_k^j is the k -th output of the j -th run. In all experiments, we set the penalty hyperparameter $\rho = 10^{12}$. Note that in (20) we only account for constraint violation only during the active learning phase, $N_i \leq k \leq N$.

The computations required to estimate NARX-NN models were performed in MATLAB 2023b on an Intel(R) Core(TM) i7-8750H CPU @ 2.20GHz with 16 GB RAM. The identification of RNN models was performed in Python 3.12 on an Intel(R) Xeon(R) W-2245 CPU @ 3.90GHz with 125 GB RAM.

4.2 Two-tank benchmark

We consider noisy synthetic data generated from a model of a two-tank system used as a nonlinear system identification benchmark in the System Identification Toolbox for MATLAB R2023b [35]. The plant model has two states (upper tank water level and lower tank water level), one output (y = lower tank water level), and one input (u = pump voltage). Samples are generated by numerically integrating the system of nonlinear ordinary differential equations of the plant model with high accuracy and collecting samples every $T_s = 0.5$ s, with initial state $x_0 = [0, 0]'$. The measurement noise is assumed to be Gaussian with zero mean and standard deviation equal to γ times the output value, i.e., $\eta_k = \gamma y_k \varepsilon_k$, where $\gamma = 0.02$, and $\varepsilon_k \sim \mathcal{N}(0, 1)$.

We use pool-based sampling with $\mathcal{U} = \{0, 0.01, \dots, 10\}$, that is, the inputs are generated by the online active learning algorithm in the interval $[0, 10]$ with resolution 0.01. When exciting the system to collect data while trying to enforce the output constraints

$$0.03 \leq y_k \leq 0.08. \quad (21)$$

We first train a two-layer NARX neural network (17),

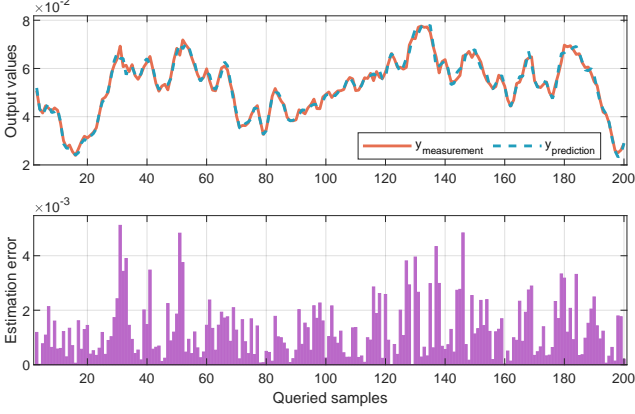


Fig. 2. Two-tank benchmark, NARX-NN model: output predictions on test data after running Algorithm 1 for N steps. Upper plot: first 200 output measurements y_k (orange line) and predictions $\hat{y}_k = f(x_{k-1}, \theta_N)$ (light blue dashed line). Lower plot: output estimation errors ($P_0 = 10^{-2}I_{n_\theta}$, $Q = 10^{-10}I_{n_\theta}$, $R = 10^{-2}I_{n_y}$).

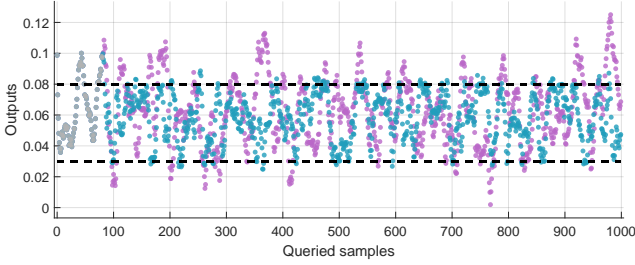


Fig. 3. Two-tank benchmark, NARX-NN model, training dataset: Initial samples (grey dots), measurements y_k without penalties (purple dots) and under soft constraints (23) (light blue dots), and constraints (21) (black dashed lines). ($P_0 = 10^{-2}I_{n_\theta}$, $Q = 10^{-10}I_{n_\theta}$, $R = 10^{-2}I_{n_y}$).

with $n_1 = 8$ and $n_2 = 6$ hidden neurons. We set the *ideal-sysid*-NARX hyperparameters, $\delta = 100$, $N_i = 80$, and $N = 1000$ and apply Algorithm 1. We also generate a test dataset of $N_{\text{test}} = 2000$ samples by simulating the system with the same initial conditions and inputs randomly sampled from the same pool \mathcal{U} .

Fig. 2 shows the one-step-ahead predicted output \hat{y}_k (upper plot) and its estimation error (lower plot) on the first 200 test data after running Algorithm 1 for N steps. The model is able to predict the output y_k accurately, with a small estimation error. Additionally, Fig. 3 shows that introducing the constraints-violation penalty term in (8) effectively prevents the outputs from violating the constraints (23) during the active input design procedure.

We compare the performance of *ideal-sysid*-NARX when the AL method, *ideal*, is replaced by GS_x , and iGS in Algorithm 1. Fig. 4 shows the RMSE and its mean absolute deviation of the predicted output y_k on test data, with and without constraints, over 30 runs. For all the considered AL methods, the RMSE values are

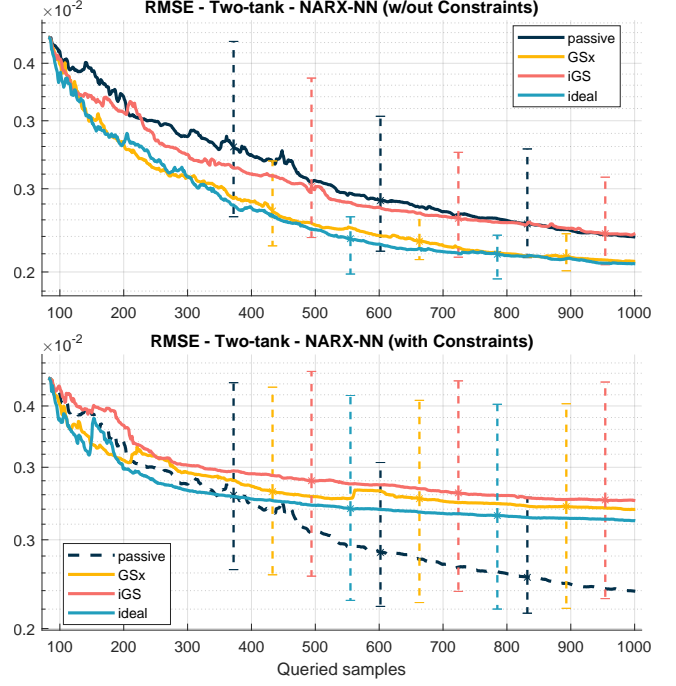


Fig. 4. Two-tank benchmark, NARX-NN model: median RMSE without constraints (upper plot) and with constraints (23) (lower plot). Constraints are not taken into account and violated by passive sampling. Vertical lines denote mean absolute deviation ($P_0 = 10^{-2}I_{n_\theta}$, $Q = 10^{-10}I_{n_\theta}$, $R = 10^{-2}I_{n_y}$).

identical for $k \leq N_i - 1$, indicating that they share the same initial randomly generated samples, resulting in the same parameters learned by the EKF. It is evident that *ideal-sysid* outperforms *passive* and iGS and is comparable to GS_x in the unconstrained case (upper plot). With constraints considered, the penalty term limits the exploration of all AL methods, *ideal-sysid* is still better than GS_x and iGS (lower plot). The *passive* method achieves the best performance because output constraints are ignored and violated. This could be observed from the MCV values in Table 1, which shows that the penalty term is effective in reducing constraint violations in all AL methods (the *passive* sampling method has more violations of the constraints). Additionally, it also shows that all AL methods better explore the output space than the *passive* method in the unconstrained case.

EKF takes between 0.118 ms and 0.562 ms (0.226 ms on average) per sample to update the NARX-NN model parameters during one run of Algorithm 1, which is negligible compared to the time required by the AL method to acquire a sample, see Table 2. Generally, the execution time of *ideal* is longer than that of GS_x and iGS , since it requires computing the IDW variance and exploration functions. The execution time of all methods is proportional to the number of elements in the pool \mathcal{U} .

Table 1

Two-tank benchmark, NARX-NN model: MCV (20) on training data. All values are in 10^{-3} units ($y_{\min} = 0.03$, $y_{\max} = 0.08$).

Model (runs)	Penalty	passive	GS _x	iGS	ideal
NARX-NN (30)	w/out	1.7	2.3	1.7	3.3
NARX-NN (30)	with	1.7	0.57	0.26	0.34
RNN (10)	w/out	1.5	1.5	2.9	1.6
RNN (10)	with	1.5	0.21	0.45	0.49

Table 2

Two-tank benchmark, NARX-NN model: running time [ms] (no penalty on output constraint violation).

Method	Min time	Avg time	Max time
passive	0.0161	0.0362	2.02
GS _x	8.74	22.8	52.7
iGS	9.57	25.2	61.5
ideal	13.1	90.8	636

As for the RNN model (18), we set $n_x = 2$, $n_y = 1$, $n_u = 1$, $n_1^x = 8$, $n_2^x = 4$, and $n_1^y = 5$. The model is initially trained by L-BFGS-B in `jax-sysid` [4] and then refined using EKF. The model parameters are updated recursively via EKF after measuring each new sample y_k . We set the `ideal-sysid-SS` hyperparameters $\delta = 1000$, $\alpha = 0.001$, $N_i = 80$, $N = 500$, and $N_{\text{test}} = 2000$, and apply Algorithm 2 over 10 runs. Fig. 5 shows that `ideal` outperforms passive sampling, similar to `GSx` and `iGS` when there are no constraints (upper plot) while with constraints `GSx` achieves the best performance (lower plot). The `passive` method performs well in the constrained case by violating output constraints, as shown in the MCV values reported in Table 1.

The execution time of EKF to update the RNN model parameters ranges between 167 ms and 1358 ms (253 ms on average) per sample in one run of Algorithm 2, while reconstructing all past states by EKF and RTS smoothing ranges between 383 ms and 1355 ms (432 ms on average). Table 3 indicates that the average execution time increases progressively across the methods, following the order `passive`, `GSx`, `iGS`, and `ideal`, as expected.

To assess the quality of the identified model after N samples are collected, we report the mean R^2 -score on the test dataset in Table 4, averaged over N_r runs. The results indicate that the learned NARX-NN and RNN models have a good accuracy. The `ideal` method consistently attains the highest R^2 values, followed by `GSx`, `iGS`, and `passive`, except in the constrained case, where `passive` performs comparably in spite of violating the output constraints. These findings are consistent with the RMSE results shown in Fig. 4 and 5 and the MCV values in Table 1.

4.3 Ethylene oxidation benchmark

We evaluate the proposed methods on the identification of an ethylene oxidation plant [10], a standard nonlin-

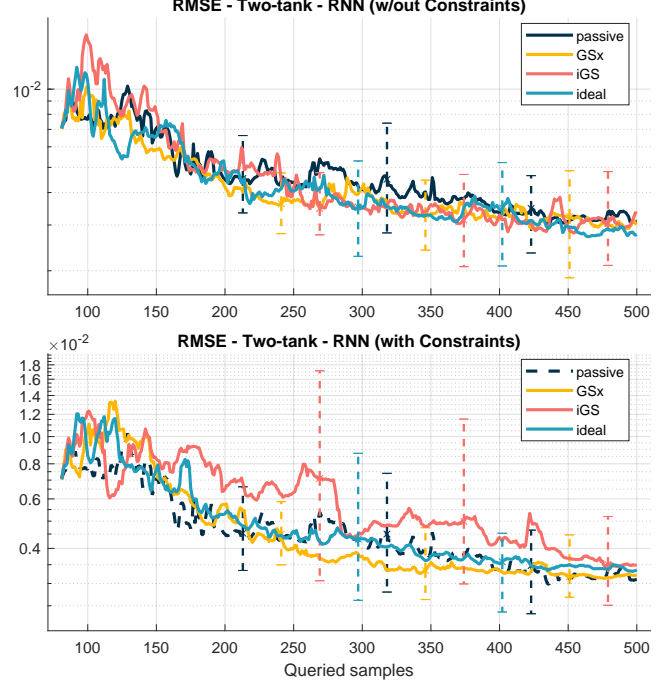


Fig. 5. Two-tank benchmark, RNN model, median RMSE: no constraints (upper plot) and with constraints (23) (lower plot). Constraints are ignored during passive sampling. Vertical lines denote mean absolute deviation ($\bar{P}_0 = \text{blockdiag}(4 \times 10^{-2} I_{n_x}, 2 \times 10^{-1} I_{(n_{\theta_x} + n_{\theta_y})})$, $\bar{Q}_x = 10^{-8} I_{n_x}$, $\bar{Q}_\theta = 10^{-8} I_{(n_{\theta_x} + n_{\theta_y})}$, $\bar{R} = I_{n_y}$).

Table 3

Two-tank benchmark, RNN model: running time [ms] (no penalty).

Method	Min time	Avg time	Max time
passive	0.125	0.180	8.46
GS _x	95.5	124	402
iGS	104	146	575
ideal	172	236	1352

Table 4

Two-tank benchmark: mean R^2 (19) (%) on test dataset

Model (runs)	Penalty	passive	GS _x	iGS	ideal
NARX-NN (30)	w/out	97.92	98.17	97.90	98.17
NARX-NN (30)	with	97.92	97.05	96.91	97.08
RNN (10)	w/out	96.67	96.64	95.50	97.24
RNN (10)	with	96.67	96.42	95.64	96.08

ear MPC benchmark from the Model Predictive Control Toolbox for MATLAB. The plant features four states (gas density, C_2H_4 concentration, $\text{C}_2\text{H}_4\text{O}$ concentration, and reactor temperature), one output ($\text{C}_2\text{H}_4\text{O}$ concentration), and two inputs: the manipulated total volumetric feed flow rate u , and a measured disturbance v (C_2H_4 feed concentration, fixed at its nominal value 0.5). Data are generated by integrating the plant's nonlinear ODEs with high accuracy, sampling every $T_s = 5$ s, and using initial conditions $x_0 = [0.9981, 0.4291, 0.0303, 1.0019]'$.

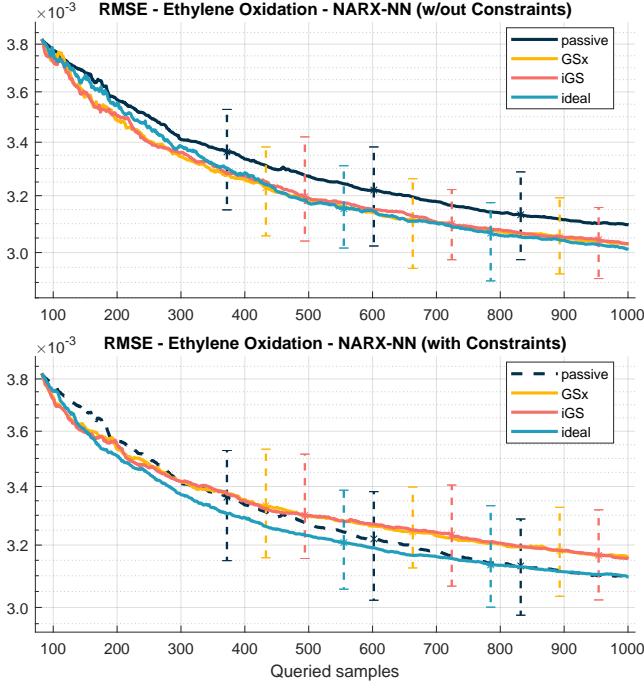


Fig. 6. Ethylene oxidation benchmark predicted by a NARX-NN model, median RMSE: no constraints (upper plot) and with constraints (22) (lower plot). Constraints are ignored during passive sampling. Vertical lines denote mean absolute deviation ($P_0 = 10^{-2}I_{n_\theta}$, $Q = 10^{-10}I_{n_\theta}$, $R = 10^{-2}I_{n_y}$).

Measurement noise $\eta_k = \gamma y_k \varepsilon_k$, with $\gamma = 0.08$, and $\varepsilon_k \sim \mathcal{N}(0, 1)$ is injected on output data. The input u is selected from the pool $\mathcal{U} = \{0.0704, 0.0804, \dots, 0.7042\}$ (step 0.01). We also consider the output constraints

$$0.02 \leq y_k \leq 0.05. \quad (22)$$

For the NARX-NN model (17), we use $n_1 = 8$, $n_2 = 6$, and set $\delta = 10$, $N_i = 80$, $N_{\text{test}} = 1000$, and apply Algorithm 1. A separate test set of $N_{\text{test}} = 2000$ samples is generated with the same initial conditions and input pool. Fig. 7 shows that all AL methods perform similarly and consistently outperform **passive** in the non-constrained case (upper plot). With constraints considered, the penalty term restricts exploration, but **ideal** remains superior to **GS_x** and **iGS**, and outperforms **passive** (lower plot). Note again that the good performance of the **passive** method is because output constraints are ignored and violated, see the MCV values in Table 5.

Then, for the RNN model (18), we set $n_x = 4$, $n_y = 1$, $n_u = 1$, $n_1^x = 8$, $n_2^x = 6$, $n_1^y = 5$, and use $\delta = 100$, $\alpha = 1$, $N_i = 100$, $N = 500$, $N_{\text{test}} = 2000$, and run Algorithm 2 10 times to collect statistics of the results.

Fig. 7 shows that AL methods are comparable and outperform passive sampling (upper plot). When con-

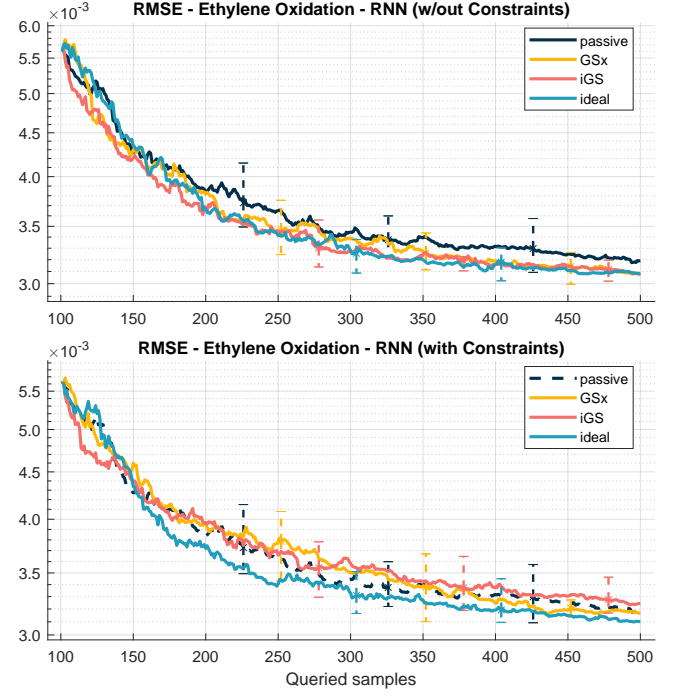


Fig. 7. Ethylene oxidation benchmark predicted by a RNN model, median RMSE: no constraints (upper plot) and with constraints (22) ($\rho = 10^6$, lower plot). Constraints are ignored during passive sampling. Vertical lines denote mean absolute deviation ($\bar{P}_0 = 2I_{(n_x+n_{\theta_x}+n_{\theta_y})}$, $\bar{Q}_x = 10^{-10}I_{n_x}$, $\bar{Q}_\theta = 10^{-10}I_{(n_{\theta_x}+n_{\theta_y})}$, $\bar{R} = I_{n_y}$).

Table 5

Ethylene oxidation benchmark: MCV (20) on training dataset. All values are in 10^{-3} units. ($y_{\min} = 0.02$, $y_{\max} = 0.05$)

Model (runs)	Penalty	passive	GS _x	iGS	ideal
NARX-NN (30)	w/out	0.71	1.4	2.1	2.7
NARX-NN (30)	with	0.71	0.33	0.28	0.59
RNN (10)	w/out	0.77	1.1	1.6	2.3
RNN (10)	with	0.77	0.41	0.42	0.64

straints are enforced, **ideal** gains the best performance (lower plot), where **passive** performs well at the expense of a violation of the constraints. This is reflected in the MCV values in Table 5.

Table 6 shows that both NARX-NN and RNN models achieve high R^2 values, though slightly lower than in the two-tank benchmark due to the higher noise level. The **ideal** method consistently yields the best R^2 performance, followed by **GS_x**, **iGS**, and **passive**. In the constrained case, **passive** can appear competitive but it disregards output constraints, as also indicated by its higher MCV values.

Table 6

Ethylene oxidation benchmark: mean R^2 (%) on test data

Model (runs)	Penalty	passive	GS _x	iGS	ideal
NARX-NN (30)	w/out	92.57	92.88	92.87	92.96
NARX-NN (30)	with	92.57	92.24	92.28	92.56
RNN (10)	w/out	92.22	92.79	92.81	92.78
RNN (10)	with	92.22	92.33	92.06	92.66

Table 7

Robot arm benchmark: MCV (20) on training dataset. All values are in 10^{-2} units. ($y_{\min} = -0.4$, $y_{\max} = 0.4$)

Model (runs)	Penalty	passive	GS _x	iGS	ideal
NARX-NN (30)	w/out	1.0	2.1	27	3.8
NARX-NN (30)	with	1.0	0.16	0.23	0.25
RNN (10)	w/out	0.91	0.94	4.8	1.8
RNN (10)	with	0.91	0.22	0.25	0.29

Table 8

Robot arm benchmark: mean R^2 (19) (%) on test dataset

Model (runs)	Penalty	passive	GS _x	iGS	ideal
NARX-NN (30)	w/out	98.16	98.55	94.74	98.62
NARX-NN (30)	with	98.16	97.35	97.40	97.54
RNN (10)	w/out	92.04	93.22	89.06	95.79
RNN (10)	with	92.04	89.94	91.73	92.65

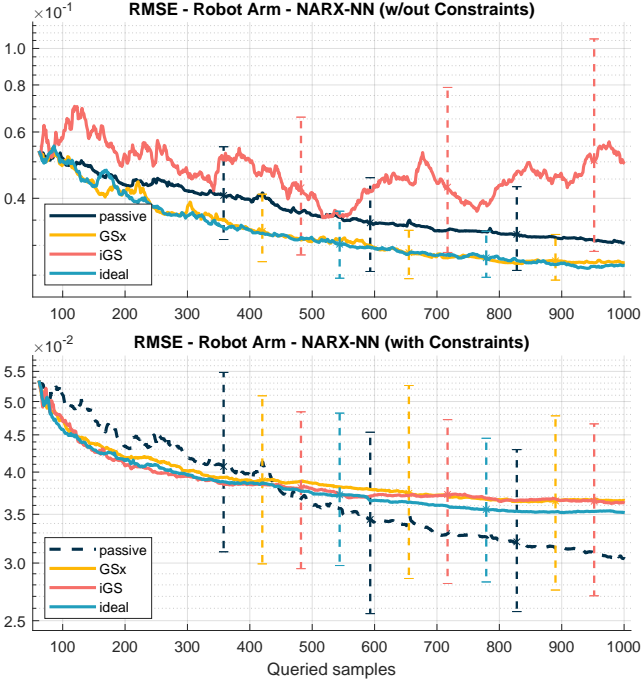


Fig. 8. Robot arm benchmark predicted by a NARX-NN model, median RMSE: no constraints (upper plot) and with constraints (23) (lower plot). Constraints are ignored during passive sampling. Vertical lines denote mean absolute deviation ($P_0 = 10^{-2}I_{n_\theta}$, $Q = 10^{-10}I_{n_\theta}$, $R = 10^{-2}I_{n_y}$).

4.4 Industrial robot arm benchmark

We evaluate the methods on the industrial robot arm benchmark [37], a nonlinear system identification problem from the System Identification Toolbox for MATLAB. The plant has five states (relative angular positions and velocities of the motor, gear-box, and arm), one output (motor angular velocity), and one input (applied motor torque). Data are generated by numerically integrating the plant's nonlinear ODEs using the adaptive stepsize Dormand-Prince Runge-Kutta method. The integration starts from the initial condition $x_0 = [0, 0, 0, 0, 0]'$, and the system output is sampled at intervals of $T_s = 0.0005$ s. Measurement noise is Gaussian with standard deviation 0.08 times the output value. The input pool is $\mathcal{U} = \{-3.0, -2.99, \dots, 3.0\}$ (step 0.01). Output constraints are set as

$$-0.4 \leq y_k \leq 0.4. \quad (23)$$

The NARX-NN (17) model has $n_1 = 16$, $n_2 = 10$ hidden neurons. We set hyperparameters $\delta = 20$, $N_i = 60$, $N_{\text{test}} = 1000$ and $N_{\text{test}} = 1000$ in Algorithm 1. Fig. 9 depicts that ideal-sysid-NARX consistently outperforms passive and iGS, and is comparable to GS_x in the unconstrained case. With exploration limited by penalty terms, ideal-sysid is still better than GS_x and iGS, and even outperforms passive before 400 samples are collected. MCV values are reported in Table 7.

The RNN model (18) is configured with $n_x = 4$, $n_y = 1$, $n_u = 1$, $n_1^x = 8$, $n_2^x = 4$, $n_1^y = 5$. We use $\delta = 1000$, $\alpha = 0.1$, $N_i = 40$, $N = 500$, $N_{\text{test}} = 2000$, and run Algorithm 2 over 10 runs. Fig. 9 shows that ideal-sysid-SS achieves the best overall performance compared to GS_x, iGS, and passive in the unconstrained case. When constraints are enforced, ideal-sysid-SS continues to perform best. The good performance of the passive method is due to ignoring output constraints, resulting in constraint violations, as reflected by the MCV values in Table 7.

Table 8 illustrates that ideal consistently yields the best R^2 performance, except in the constrained case, where, in spite of violating output constraints, passive performs comparably.

5 Conclusion

We have presented and compared several active learning methods for online design of experiments tailored to the identification of nonlinear dynamical systems from input/output data, both in autoregressive and state-space form. By combining ideas of active learning for regression with recursive parameter estimation based on Kalman filtering, we demonstrated improved sample efficiency

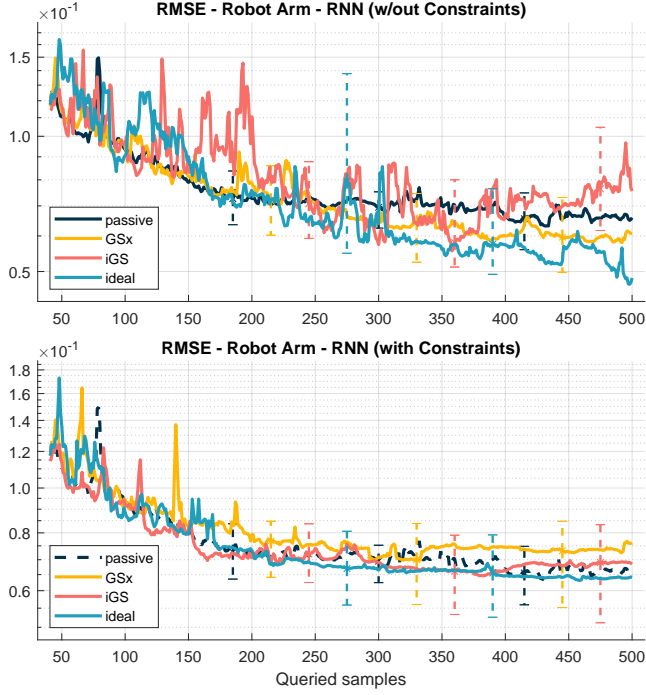


Fig. 9. Robot arm benchmark predicted by a RNN model, median RMSE: no constraints (upper plot) and with constraints (23) (lower plot). Constraints are ignored during passive sampling. Vertical lines denote mean absolute deviation ($\bar{P}_0 = \text{diag}(2 \times 10^{-1} I_{n_x}, 2 \times 10^{-2} I_{(n_{\theta_x} + n_{\theta_y})})$, $\bar{Q}_x = 10^{-8} I_{n_x}$, $\bar{Q}_\theta = 10^{-8} I_{(n_{\theta_x} + n_{\theta_y})}$, $\bar{R} = 6.4 \times 10^{-3} I_{n_y}$).

across a range of benchmark problems, as well as the ability of considering output constraints. All the proposed AL strategies provide benefits compared to standard random excitation. Among them, the ideal-sysid approach exhibited a robust and consistent performance. The results highlight the advantages of incorporating both exploration and exploitation terms in the acquisition function to ensure informative and diverse data collection. Future work will address the integration of these active learning strategies with closed-loop control, such as model predictive control.

Acknowledgments

The authors would like to thank Sampath Kumar Mulagaleti for fruitful discussions.

References

- [1] C.C. Aggarwal, X. Kong, Q. Gu, J. Han, and P.S. Yu. Active learning: A survey. In C.C. Aggarwal, editor, *Data Classification: Algorithms and Applications*, chapter 22, pages 572–605. Chapman and Hall/CRC Press, 2014.
- [2] A. Bemporad. Active learning for regression by inverse distance weighting. *Information Sciences*, 626:275–292, 2023. Code available at <http://cse.lab.imtlucca.it/~bemporad/ideal>.
- [3] A. Bemporad. Recurrent neural network training with convex loss and regularization functions by extended Kalman filtering. *IEEE Transactions on Automatic Control*, 68(9):5661–5668, 2023.
- [4] A. Bemporad. An L-BFGS-B approach for linear and nonlinear system identification under ℓ_1 and group-lasso regularization. *IEEE Transactions on Automatic Control*, pages 1–8, 2025.
- [5] R. Burbidge, J.J. Rowland, and R.D. King. Active learning for regression based on query by committee. In *Proc. Int. Conf. on Intelligent Data Engineering and Automated Learning*, pages 209–218, 2007.
- [6] R.H. Byrd, P. Lu, J. Nocedal, and C. Zhu. A limited memory algorithm for bound constrained optimization. *SIAM Journal on Scientific Computing*, 16(5):1190–1208, 1995.
- [7] W. Cai, Y. Zhang, and J. Zhou. Maximizing expected model change for active learning in regression. In *Proc. IEEE Int. Conf. on Data Mining (ICDM)*, pages 51–60, 2013.
- [8] R. Chin, A.I. Maass, N. Ulapane, C. Manzie, I. Shames, D. Nešić, J.E. Rowe, and H. Nakada. Active learning for linear parameter-varying system identification. *IFAC-PapersOnLine*, 53(2):989–994, 2020.
- [9] D.A. Cohn, Z. Ghahramani, and M.I. Jordan. Active learning with statistical models. *Journal of Artificial Intelligence Research*, 4:129–145, 1996.
- [10] H. Durand, M. Ellis, and P.D. Christofides. Economic model predictive control designs for input rate-of-change constraint handling and guaranteed economic performance. *Computers & Chemical Engineering*, 92:18–36, 2016.
- [11] R.A. Fisher. *The Design of Experiments*. Oliver & Boyd, Edinburgh, 1935.
- [12] H. He, A. Tran, D.M. Bortz, and Y. Choi. Physics-informed active learning with simultaneous weak-form latent space dynamics identification. *International Journal for Numerical Methods in Engineering*, 126(1):e7634, 2024.
- [13] U.J. Islam, K. Paynabar, G. Runger, and A.S. Iquebal. Dynamic exploration–exploitation trade-off in active learning regression with Bayesian hierarchical modeling. *IIEE Transactions*, 57(4):393–407, 2024.
- [14] V. Roshan Joseph and L. Kang. Regression-based inverse distance weighting with applications to computer experiments. *Technometrics*, 53(3):254–265, 2011.
- [15] M. Kiss, R. Tóth, and M. Schoukens. Space-filling input design for nonlinear state-space identification. arXiv preprint arXiv:2405.18207, 2024.
- [16] J. Knaup and P. Tsiotras. Adaptive dual covariance steering with active parameter estimation. In *Proc. 63rd IEEE Conf. on Decision and Control*, pages 659–664, Milan, Italy, 2024.
- [17] P. Kumar and A. Gupta. Active learning query strategies for classification, regression, and clustering: A survey. *Journal of Computer Science and Technology*, 35(4):913–945, 2020.
- [18] B. Lee, I. Ziemann, G.J. Pappas, and N. Matni. Active learning for control-oriented identification of nonlinear systems. In *Proc. 63rd IEEE Conf. on Decision and Control*, pages 3011–3018, Milan, Italy, 2024.
- [19] T.-C. Lee, Y. Tan, and D. Nešić. Stability and persistent excitation in signal sets. *IEEE Transactions on Automatic Control*, 60(5):1188–1203, 2015.
- [20] Z. Liu, X. Jiang, H. Luo, W. Fang, J. Liu, and D. Wu. Pool-based unsupervised active learning for regression using iterative representativeness-diversity maximization (iRDM). *Pattern Recognition Letters*, 142:11–19, 2021.

- [21] L. Ljung. Asymptotic behavior of the extended Kalman filter as a parameter estimator for linear systems. *IEEE Transactions on Automatic Control*, 24(1):36–50, 1979.
- [22] L. Ljung. *System Identification (2nd ed.): Theory for the User*. Prentice Hall PTR, Upper Saddle River, NJ, 1999.
- [23] L. Ljung, C. Andersson, K. Tiels, and T.B. Schön. Deep learning and system identification. *IFAC-PapersOnLine*, 53(2):1175–1181, 2020. 21st IFAC World Congress.
- [24] E.T.B. Lundby, A. Rasheed, I.J. Halvorsen, D. Reinhardt, S. Gros, and J.T. Gravdahl. Deep active learning for nonlinear system identification. arXiv preprint arXiv:2302.12667, 2023.
- [25] D.J.C. MacKay. Information-based objective functions for active data selection. *Neural Computation*, 4(4):590–604, 1992.
- [26] I.M.Y. Mareels and M. Gevers. Persistency of excitation criteria for linear, multivariable, time-varying systems. *Mathematics of Control, Signals and Systems*, 1(3):203–226, 1988.
- [27] G. Pillonetto, A. Aravkin, D. Gedon, L. Ljung, A.H. Ribeiro, and T.B. Schön. Deep networks for system identification: A survey. *Automatica*, 171:111907, 2025.
- [28] T. RayChaudhuri and L.G.C. Hamey. Minimisation of data collection by active learning. In *Proc. Int. Conf. on Neural Networks*, volume 3, pages 1338–1341, 1995.
- [29] R. Rickenbach, J. Köhler, A. Scampicchio, M.N. Zeilinger, and A. Carron. Active learning-based model predictive coverage control. *IEEE Transactions on Automatic Control*, pages 1–16, 2024.
- [30] C.R. Rojas, J.S. Welsh, G.C. Goodwin, and A. Feuer. Robust optimal experiment design for system identification. *Automatica*, 43(6):993–1008, 2007.
- [31] S. Särkkä and L. Svensson. *Bayesian Filtering and Smoothing*, volume 17. Cambridge University Press, 2023.
- [32] B. Settles. *Active Learning*. Synthesis Lectures on Artificial Intelligence and Machine Learning. Morgan & Claypool, 2012.
- [33] Ö. Sürer. Simulation experiment design for calibration via active learning. *Journal of Quality Technology*, 57(1):16–34, 2024.
- [34] S. Tang, K. Fujimoto, and I. Maruta. Actively learning Gaussian process dynamical systems through global and local explorations. *IEEE Access*, 10:24215–24231, 2022.
- [35] The MathWorks, Inc. *Two-Tank System: C-MEX-File Modeling of Time-Continuous SISO System*. MATLAB System Identification Toolbox, 2020.
- [36] A.M. Vepa, Z. Yang, A. Choi, J. Joo, F. Scalzo, and Y. Sun. Integrating deep metric learning with coresets for active learning in 3D segmentation. In *Proc. 38th Int. Conf. on Neural Information Processing Systems*, page 2288, Vancouver, BC, Canada, 2024.
- [37] E. Wernholt and S. Gunnarsson. Nonlinear identification of a physically parameterized robot model. *IFAC-PapersOnLine*, 39(1):143–148, 2006. 14th IFAC Symposium on Identification and System Parameter Estimation.
- [38] D. Wu, C.-T. Lin, and J. Huang. Active learning for regression using greedy sampling. *Information Sciences*, 474:90–105, 2019.
- [39] K. Xie and A. Bemporad. Online design of experiments by active learning for system identification of autoregressive models. In *Proc. 63rd IEEE Conf. on Decision and Control*, pages 7202–7207, Milan, Italy, 2024.
- [40] J. Yang, R.G. Lal, J.C. Bowden, R. Astudillo, M.A. Hameedi, S. Kaur, M. Hill, Y. Yue, and F.H. Arnold. Active learning-assisted directed evolution. *Nature Communications*, 16(1):714, 2025.
- [41] H. Yu and S. Kim. Passive sampling for regression. In *Proc. IEEE Int. Conf. on Data Mining*, pages 1151–1156, 2010.
- [42] H.S.A. Yu, C. Zimmer, and D. Nguyen-Tuong. Batch active learning in Gaussian process regression using derivatives. arXiv preprint arXiv:2408.01861, 2024.